View Article Online / Journal Homepage / Table of Contents for this issue
Dynamic Article Links

Energy & Environmental Science

Cite this: *Energy Environ. Sci.*, 2011, **4**, 2870

www.rsc.org/ees

PAPER

Morphosynthesis of a hierarchical MoO_2 nanoarchitecture as a binder-free anode for lithium-ion batteries†

Yongming Sun,[a] Xianluo Hu,*[a] Jimmy C. Yu,[b] Quan Li,[c] Wei Luo,[a] Lixia Yuan,[a] Wuxing Zhang[a] and Yunhui Huang*[a]

Received 17th February 2011, Accepted 3rd May 2011
DOI: 10.1039/c1ee01189h

Published on 17 June 2011. Downloaded by Chinese University of Hong Kong on 26/09/2013 08:19:55.

A simple and cost-effective morphogenetic route has been developed for the fabrication of a hierarchically nanostructured "cellulose" MoO_2 monolith in large qualities, whereby the cotton texture acts as both a template and a stabilizer. The MoO_2 monolith possesses hierarchical porosity and an interconnected framework, which is demonstrated to be useful as a binder-free anode in rechargeable lithium-ion batteries with both high specific capacity of 719.1 mA h g^{-1} and good reversibility. Our single-component anode for lithium-storage devices also benefits from a simplified fabrication process and reduced manufacturing cost, in comparison with conventional multicomponent electrodes that are fabricated from a mixture of polymer binders and active materials. The present morphogenetic strategy is facile but effective, and therefore it is very promising for large-scale industrial production. It can be extended to prepare other metal oxides with elaborate textural characteristics.

Introduction

New materials hold the key to fundamental advances in energy conversion and storage for addressing the challenges of global warming and energy crisis. Much effort has been particularly devoted to fabricating a great number of nanostructured materials as electrodes in a range of lithium-ion batteries.[1] This research trend has been evidenced by many interesting pioneering works published during the past decade.[2] As expected, the nanostructuring of electrode materials leads to reduced solid-state diffusion lengths for both Li^+ and e^- because of the confining dimension effect, increased charge capacity due to their high surface area, and eventually enhanced collective performance of lithium-ion batteries with higher power and energy density.[3] In particular, materials with hierarchically nanostructured frameworks are highly attractive in lithium-ion batteries because of their high porosity, high surface area, and excellent performance (*e.g.*, enhanced cyclability).[4] While studies are actively being pursued on a variety of inorganic nanostructured metals and metal oxides as electrode materials in lithium-ion batteries, little work exists towards the

[a]*State Key Laboratory of Material Processing and Die & Mould Technology, School of Materials Science and Engineering, Huazhong University of Science and Technology, Wuhan, 430074, P. R. China. E-mail: huxl@mail.hust.edu.cn; huangyh@mail.hust.edu.cn; Tel: +86-27-87558241*
[b]*Department of Chemistry, The Chinese University of Hong Kong, Shatin, New Territories, Hong Kong, P. R. China*
[c]*Department of Physics, The Chinese University of Hong Kong, Shatin, New Territories, Hong Kong, P. R. China*

† Electronic supplementary information (ESI) available: XRD, SEM, XPS, TG/DTA, FT-IR, and electrochemical analyses. See DOI: 10.1039/c1ee01189h/

Broader context

Rechargeable lithium-ion batteries (LIBs) have long been explored as an increasingly important power source for a wide variety of applications including portable electronic devices, implantable medical devices, and electric vehicles. So far, significant efforts have been devoted to designing, fabricating, and engineering various LIB materials with high reversible capacity, long cycle life, and low cost. Nanostructuring of electrode materials may lead to reduced solid-state diffusion lengths for both Li^+ and e^-, increased charge capacity, and enhanced collective performance of LIBs with higher power and energy density. In particular, the electrode materials with hierarchically nanostructured frameworks are highly attractive for LIBs because of their high porosity and high surface area. Here we describe a cost-effective morphogenetic strategy to fabricate a hierarchically nanostructured "cellulose" MoO_2 monolith in large qualities. The combination of unique macroscopically patterned nanostructures, inter-nanocrystallite and porosity, and large internal surfaces makes the resulting "cellulose" MoO_2 monolith an ideal candidate as a binder-free anode for lithium-storage applications.

 This journal is © The Royal Society of Chemistry 2011

Published on 17 June 2011. Downloaded by Chinese University of Hong Kong on 26/09/2013 08:19:55.

morphosynthesis of electrochemically active, hierarchically nanoarchitectured monoliths with precise multi-scale control. Efficient methods are much needed for the fabrication of novel nanostructured monolithic materials, for instance, as binder-free electrodes for rechargeable lithium batteries.[5]

Morphosynthesis consists of the chemical construction and patterning of inorganic materials with unusual and complex architectures at different length scales.[6] In fact, nature has ever fascinated scientists and engineers with numerous examples of exceptional building materials. These materials often possess complex hierarchical configuration from the nanometre to the macroscopic scale.[7] Based on bottom-up self-assembly processes,[8] a wide variety of organisms have been found to be capable of growing nanostructured inorganic components into functional inorganic nanomaterials with complex architectures on flexible length scales that cannot be exactly achieved by traditional processing technologies.[9] Taking MoO_2 as an example, here we present the use of commercial cotton textile, a natural cellulose derivation, as both the template and the stabilizer for the morphosynthesis of hierarchically porous MoO_2 nanoarchitectures *via* a mild impregnation process followed by calcination in air and H_2/Ar. Scheme 1 illustrates the formation process of hierarchical MoO_2 nanostructures. Three major processes are involved: impregnation, decomposition, and reduction.

Molybdenum oxides (MoO_x) have received much attention as host substances for lithium insertion owing to their rich chemistry associated with multiple valence states, low electrical resistivity, high stability, and affordable cost.[10] Several synthetic approaches have been reported for preparing well-defined MoO_x nanostructures including (i) nanoparticles,[11] nanosheets,[12] hybrids[13] and mesoporous structures of MoO_2,[14] and (ii) nanoparticles,[15] nanorods,[16] nanobelts,[17] nanosheets,[18] and hybrids of MoO_3.[19] The fabrication of complex monolithic MoO_x architectures, particularly with hierarchically nanostructured patterns in a macroscopic length, has never been reported. In particular, complex hierarchical architectures of MoO_x over multiple scales would hold great promise for use in lithium storage devices. This work reports for the first time on a novel MoO_2 monolith that is utilized as a binder-free alternative anode to conventional MoO_2-based electrodes that are fabricated from the mixture of a polymer binder and an active material. When evaluated as an anode material for lithium-ion batteries, the as-formed MoO_2 monolith with a hierarchically porous configuration exhibits a high reversible lithium-storage capacity of 719.1 mA h g^{-1}.

Experimental

Materials synthesis

All chemicals were used as received without further purification. Deionized (DI) water was used throughout. Cotton cloth was collected from the general market and cleaned with DI water. In a typical synthesis, phosphomolybdic acid (PMA, $H_3PMo_{12}O_{40}\cdot xH_2O$, 1 mmol) was dissolved into ethanol (10 mL) at room temperature to form an homogeneous solution under stirring. A piece of cotton cloth (0.2 g) was cut and immersed into the solution. After stirring for 2 h, the cotton cloth was taken out, dried at 60 °C for 5 min in a preheated oven, and cured at 90 °C for 3 h. The obtained PMA/cotton cloth hybrid was calcined at 600 °C in air for 4 h to generate MoO_3. The as-formed product was subsequently treated at 600 °C (ramp rate: 1 °C min^{-1}) in a 5% H_2/Ar atmosphere for 5 h. Finally, the black-coloured product of MoO_2 was collected for further characterizations.

Materials characterization

X-ray diffraction (XRD) patterns were collected using a X'Pert PRO (PANalytical B.V., Holland) diffractometer with high-intensity Cu $K_{\alpha 1}$ irradiation (λ = 1.5406 Å). The accelerating voltage and the applied current were 40 kV and 40 mA, respectively. The general morphology of the products was characterized by field-emission scanning electron microscopy (FE-SEM, FEI, Sirion 200) coupled with an energy-dispersive X-ray (EDX, Oxford Instrument) spectrometer. Transmission electron microscopy (TEM) observations were carried out on a JEM-2100F microscope (JEOL). The thermogravimetric (TG) analysis and differential thermal analysis (DTA) were performed with a PerkinElmer Diamond TG/DTA apparatus. TG and DTA were measured simultaneously at a heating rate of 10 °C min^{-1} in flowing air. X-ray photoelectron spectroscopy (XPS) measurements were performed on a VG MultiLab 2000 system with a monochromatic Al Kα X-ray source (ThermoVG Scientific). Infrared spectra were recorded using a Bruker VERTEX 70 FT-IR spectrometer.

Electrochemical measurement

The electrochemical behavior of the as-formed MoO_2 product, as a proposed binder-free anode in lithium-ion batteries, has been investigated in typical coin cells (half-cells). The coin cells were

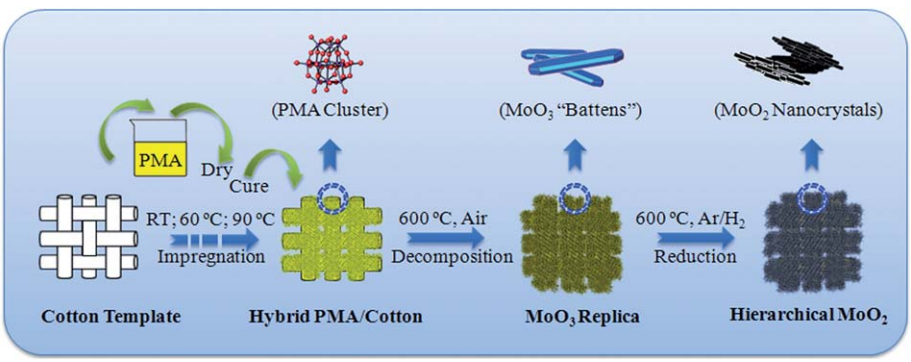

Scheme 1 Schematic illustration of hierarchical MoO_2 formation.

Published on 17 June 2011. Downloaded by Chinese University of Hong Kong on 26/09/2013 08:19:55.

laboratory-assembled by a CR2032 press in an argon-filled glovebox where moisture and oxygen concentrations were strictly limited to below 1 ppm. A lithium foil was used as the counter electrode, and a Celgard 2300 membrane was used as the separator. A piece of hierarchically nanostructured MoO_2 monolith was dried in a vacuum at 80 °C for 24 h, and used directly as the working electrode without any polymeric binder involved. The commercial electrolyte was composed of 1 mol L^{-1} $LiPF_6$ in a mixture of ethylene carbonate (EC) and dimethyl carbonate (DMC) (v/v = 1 : 1). Cyclic voltammetry (CV) curves were recorded on a PARSTAT 2273 potentiostat at a scanning rate of 0.1 mV s^{-1} at room temperature. The galvanostatic charge-discharge tests were carried out on a Land Battery Measurement System (Land, China) at a current density of 200 mA g^{-1} with a cutoff voltage of 3.00–0.01 V *vs.* Li/Li^+ at room temperature.

Results and discussion

Cotton has been used by mankind for at least 7000 years.[20] Nowadays, the production of cotton worldwide is approximately 20 million tons per annum, mainly for clothing, paper, and medical applications. As the oldest and most commonly used nanoporous material, it is constructed from polysaccharide chains arranged into crystalline and amorphous regions, where the amorphous regions are slit pores of a few nanometres in width and are sandwiched between crystallites.[20] Knitted cotton fabric such as terry cloth is cheap and widely available for constructing new materials and immobilizing biomolecules.[21] Activated with a variety of reagents (*e.g.*, CNBr, sulfonyl chlorides, and periodate), cotton fibers made of a cellulose backbone can form a covalent bond with enzymes.[22] In this study, the primary hydroxyl groups of cellulose in cotton cloth may react with PMA in a nonaqueous solvent through an esterification mechanism to produce an homogeneous PMA/cotton composite.[22] As illustrated in Scheme 1, a sheet of cotton cloth made of natural cellulose was firstly immersed in a polyoxometalate (POM) solution of PMA. Then, the freshly formed POM/cotton hybrid was converted into a crystalline hierarchical MoO_3 replica through a thermal-treatment process at 600 °C for 4 h in air. The cellulose fiber was removed during the process, and the MoO_3 replica maintained the original configuration of the cloth template. Eventually, a hierarchically nanoparticle-organized MoO_2 monolith was formed *in situ* by reduction of Mo(VI) to Mo (IV) at 600 °C for 5 h in a 5% H_2/Ar atmosphere. The as-formed MoO_2 monolith is relatively robust for subsequent processing. The digital camera images of the cotton template, hybrid PMA/cotton, and hierarchical MoO_2 are shown in Fig. S1 (see ESI†). This present strategy may allow for easy control of the scale and microstructure of the final MoO_2 product because the original cellulose templates could be well "spun", "woven" and "tailored" *via* state-of-the-art textile fabrication techniques. This strategy is also highly promising for the large-scale industrial production of MoO_2 nanostructures with tunable hierarchical patterns serving as electrode materials for energy conversion and storage devices.

Powder XRD patterns provide crystallinity and phase information for the products. The results indicate that the intermediate obtained through the decomposition and combustion of the cotton/PMA hybrid in air is pure orthorhombic MoO_3 (JCPDS No. 35-0609, Fig. S2, ESI†). Fig. 1a shows the representative XRD pattern for the final MoO_2 product prepared by reducing the MoO_3 replica at 600 °C for 5 h in a 5% H_2/Ar atmosphere. All the diffraction peaks are readily indexed to a pure monoclinic phase [space group: $P2_1/c$ (14)] of MoO_2 (JCPDS No. 65-5787; a = 5.6109 Å, b = 4.8562 Å, c = 5.6285 Å; β = 120.95°). No characteristic peaks were observed for impurities such as phosphates and MoO_3 as well as other kinds of molybdenum oxides. Important information on the surface electronic state and the composition of the final product can be further provided by XPS. The binding energies obtained in the XPS analysis were corrected for specimen charging by referencing the C 1s line to 284.5 eV. A typical survey XPS spectrum for the MoO_2 product (Fig. 1b) involves four distinct peaks at 233.9 (Mo 3d), 398.0 (Mo $3p_{3/2}$), 415.6 (Mo $3p_{1/2}$), and 531.9 (O 1s) eV, characteristic of molybdenum oxides.[23] The Mo 3d peak was further examined by high-resolution XPS (Fig. S3, see ESI†). The Mo $3d_{5/2}$ peak is centered at 229.3 eV whereas the Mo $3d_{3/2}$ peak is found at 232.4 eV, with a spin energy separation of 3.1 eV. This characteristic doublet of core-level Mo $3d_{5/2,3/2}$ indicates the Mo(IV) oxidation state of MoO_2.[23] In addition, a peak at 235.6 eV could be ascribed to Mo (VI) $3d_{3/2}$ of MoO_3, arising from the slight surface oxidation of the metastable MoO_2 in air.[11a]

Representative FE-SEM images of the products are shown in Fig. 2. The original cloth used in this work is actually an artificial pseudo-2D network of cotton threads in compact bundles through simple weaving (Fig. 2a). Each bundle comprises many strips with an average diameter of ~10 μm. After impregnation of PMA clusters and subsequent calcination at 600 °C for 4 h in air, the obtained MoO_3 product exhibits perfect replication of the configuration from the original cloth network (Fig. 2b). Interestingly, close observation confirms that a great number of

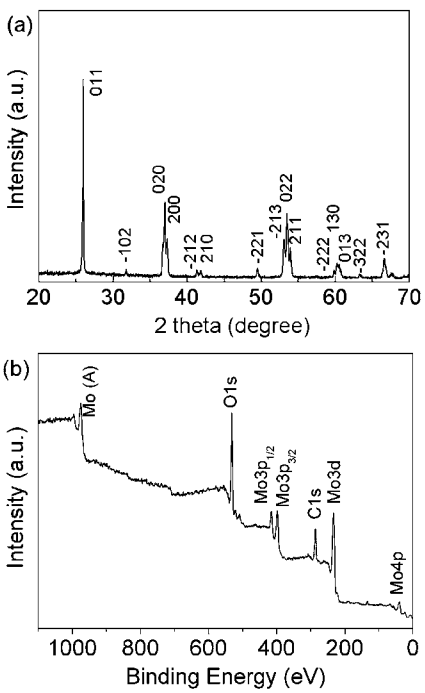

Fig. 1 (a) Representative XRD pattern of the MoO_2 product prepared by reducing MoO_3 replica at 600 °C for 5 h in 5% H_2/Ar. (b) Survey XPS spectrum of the as-formed hierarchically structured MoO_2.

 This journal is © The Royal Society of Chemistry 2011

Published on 17 June 2011. Downloaded by Chinese University of Hong Kong on 26/09/2013 08:19:55.

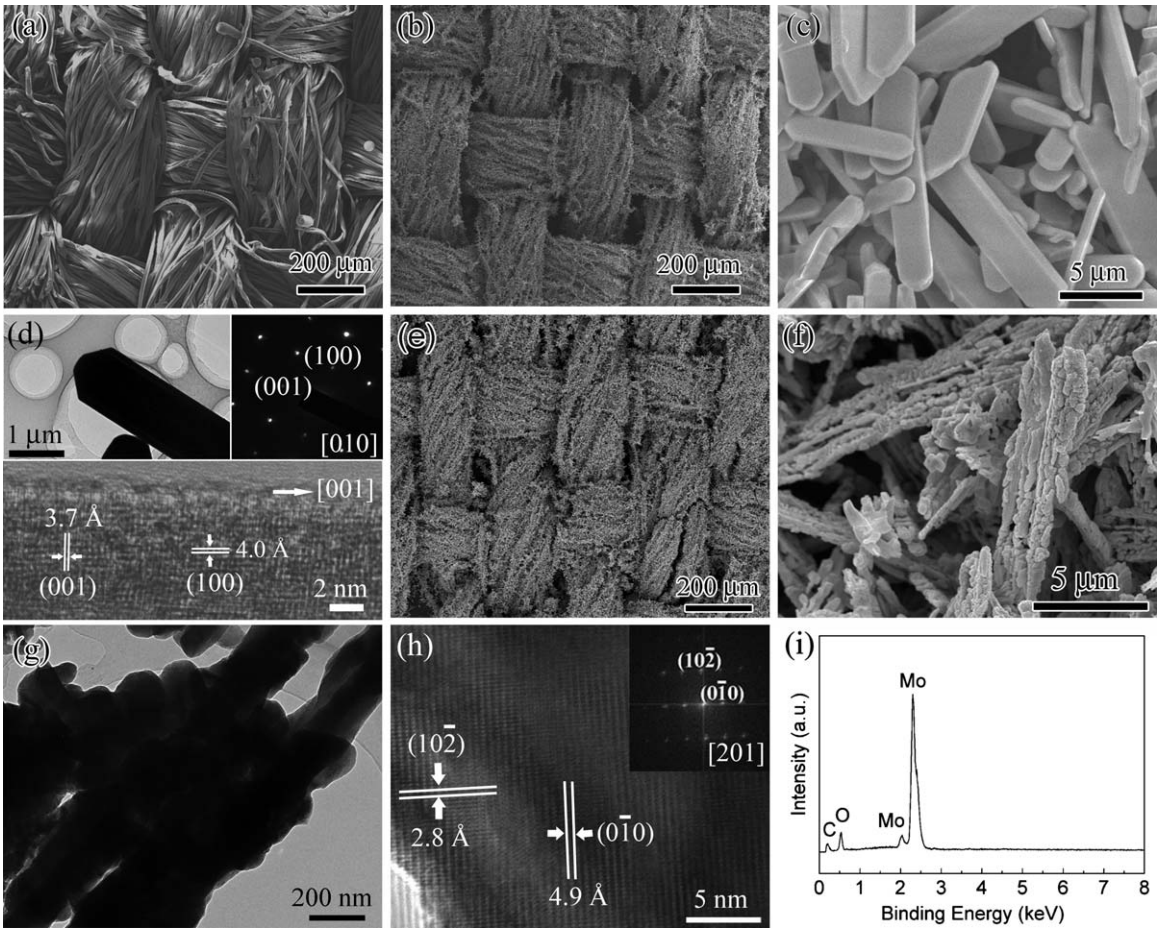

Fig. 2 (a) Low-magnification FE-SEM image of the original cloth template. (b,c) FE-SEM images of the MoO_3 replica obtained at 600 °C for 4 h in air. (d) TEM image of a single MoO_3 "batten". Inset: ED pattern indicating the single-crystal nature of the "batten" (upright); HRTEM image (bottom). Representative SEM (e,f) and TEM (g) images of the MoO_2 product obtained at 600 °C for 5 h in H_2/Ar, indicating a hierarchically porous architecture. (h) Typical HRTEM image and the corresponding fast Fourier-transform (FFT) pattern (inset) taken from a MoO_2 nanocrystal. (i) EDX spectrum of the MoO_2 product, where the signal of C is generated from the sample holder.

batten-like crystallites are formed with well-defined and smooth facets (Fig. 2c), serving as building blocks to construct a typical hierarchical patterning. The dimensions are in the range of 5–15 μm in length, 1–4 μm in width, and 100–500 nm in thickness. TEM and HRTEM images provide further insight into structural information on the secondary structure composed of MoO_3 batten-like crystallites. Fig. 2d shows a typical bright-field TEM image for an individual batten with a length of ~8 μm and a width of ~1 μm. Its corresponding selected area electron diffraction (SAED) pattern is shown in the top-right inset of Fig. 2d. It can be indexed to the [010] zone axis of the orthorhombic-structured MoO_3. Experiments show that the SAED patterns on different "battens" or different positions of a given single "batten" were essentially identical, which indicates that the MoO_3 "battens" are single-crystalline in nature. The fringes in a typical HRTEM image (at the bottom of Fig. 2d) are separated by ~4.0 Å, which agrees well with the {100} lattice spacing of the orthorhombic MoO_3. This indicates that MoO_3 "micro-battens" had preferential two-dimensional (2D) growth directions along [001] and [100] of the crystal lattice.

The MoO_3 "micro-battens" could be reduced to MoO_2 by thermal hydrogen reduction. The size and thickness of the monolith would depend on the original cloth used, and therefore could be controlled easily by "weaving" and "tailoring" of the original cellulose templates. Fig. 2e shows the general morphology for the final MoO_2 product, indicating that it has a similar hierarchical topology to that of the MoO_3 replica. Very interestingly, each original batten-like single microcrystal has evolved into an assembly comprising a great number of tiny MoO_2 grains of 10–50 nm that align crystallographically in a specific orientation, leading to the formation of a nanoporous framework (Fig. 2f). Fig. 2g displays a typical TEM image of MoO_2 nanocrystals that evolved from an individual father "batten" of MoO_3. Fig. 2h shows the HRTEM image taken from the edge of an individual MoO_2 nanoparticle, which provides more detailed structural information on these nanoparticles. The periodic fringe spacing of ~4.9 Å agrees well with interplanar spacing between the {0$\bar{1}$0} planes of the monoclinic MoO_2. The crystalline monoclinic structure is also mirrored in the fast Fourier transform (FFT) pattern shown in the inset of Fig. 2h. EDX microanalysis (Fig. 2i) confirms that the nanocrystals are composed of Mo and O, which is consistent with the XPS and XRD results (Fig. 1).

The influence of reaction temperature on the morphology and composition of the products was investigated. When the

Published on 17 June 2011. Downloaded by Chinese University of Hong Kong on 26/09/2013 08:19:55.

calcination temperature was lower than 400 °C, the phase of the product revealed by XRD was not crystalline MoO_3 anymore. Verified by TG/DTA analysis, the decomposition of pure PMA to MoO_3 indeed occurs at a temperature of higher than 400 °C (Fig. S4, see ESI†). At calcination temperatures ranging from 450 to 500 °C, no "battens" but only irregular sub-micrometre MoO_3 particles were formed (Fig. S5, see ESI†). Also, the macroscopic patterned configuration was not well replicated from the cotton template, and evident deformation and collapse somewhere in the framework appeared. At the optimized temperature of 600 °C, well-defined hierarchical patterning of MoO_3 "battens" was achieved (Fig. 2b and 2c). TG/DTA results reveal that the decomposition of PMA and removal of cotton are completely carried out at 600 °C (Fig. S6, ESI†). However, larger MoO_3 crystallites could be observed when the calcination temperature was further increased. In a control experiment, we obtained a MoO_2 sample directly by the same two-step procedure of decomposition in air and reduction in 5% H_2/Ar without using any cotton template. FE-SEM images show that the resulting MoO_2 sample is composed of irregular-shaped particles with a broad size distribution of 0.5–5 μm (Fig. S7, ESI†). Obviously, the cotton texture functions not only as the template but also as a stabilizer in the formation of the "batten"-organized patterning. As displayed in the FT-IR spectrum (Fig. S8, ESI†), the cotton template possesses plenty of functional groups such as OH and C=O that are highly beneficial for a bottom-up-type self-assembly of PMA on the template surface.[8] It was found that the reduction of MoO_3 "battens" to assembled MoO_2 nanocrystals should be carried out at a minimum temperature of 500 °C in order to form a pure phase of MoO_2. The optimal PMA concentration for the impregnation process was found to be 0.1 mol L^{-1}. These results suggest that it is feasible to achieve well-defined hierarchically structured MoO_2 nanoarchitectures by controlling the reaction temperature as well as the concentration of the POM precursor solution.

It is well known that POMs are anionic metal oxide clusters with a polynuclear metal-oxo structure, and are widely exploited as versatile inorganic building blocks for constructing functional hybrid materials. They can also be viewed as an array of MO_x polyhedral units (*e.g.*, M = Mo^{VI}, W^{VI}, V^{V}; x = 4–7) linked *via* edge, corner, and occasionally face sharing modes.[24] We chose PMA (a typical POM) with a cluster diameter of approximately 1 nm as the molybdenum source, as schematically depicted in Fig. 3a. Since cellulose fibers of cotton are highly porous and readily accessible to external agents,[25] PMA tends to be impregnated into the template through stirring of the cellulose template in PMA solution. After the traditional drying and curing procedures, a POM/template hybrid is formed, in which the cotton template also functions as a stabilizer. This route belongs to the general "nanocasting" method and is closely related to the sol–gel process. Subsequently, small POM clusters are decomposed to generate MoO_3 nuclei by heating treatment at 600 °C in air. Meanwhile, the freshly formed nanocrystals are unstable due to their high surface energy, and thus they have a great tendency to aggregate and grow into MoO_3 microcrystallites with well-defined shapes (Fig. 2b and 2c). The cotton template combusts during the heating process, and the resulting heat release prompts the above aforementioned crystal growth. As evidenced by SAED and HRTEM results (Fig. 2d), the

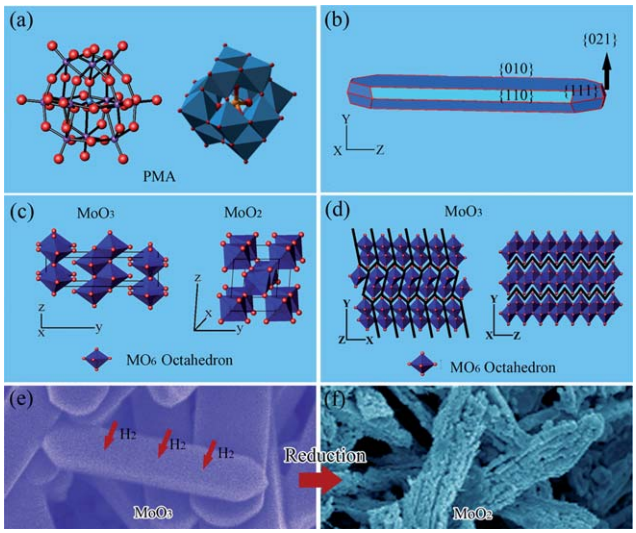

Fig. 3 (a) Molecular structures of PMA. (b) Structural mode of a truncated batten-like shape. (c) Unit cells of the orthorhombic phase of MoO_3 (left) and the monoclinic phase of MoO_2 (right). (d) Crystal models of orthorhombic MoO_3 projected along [001] and [100]. (e,f) Schematic illustration for the transformation from MoO_3 "battens" into porous MoO_2 nanocrystal assemblies.

batten-like crystal of MoO_3 was proven to grow along the [001] and [100] directions. The exposed planes are dominated by (010) planes as well as their equivalent $(0\bar{1}0)$ planes. As depicted in Fig. 3b, the as-grown shape of MoO_3 crystals (Fig. 2c) matches very well with the "batten" model that is enclosed with {010}, {110}, {111}, and {021} faces. Such a growth habit may be attributed to the intrinsic nature of orthorhombic MoO_3. In general, the fast-growing planes are eliminated quite rapidly, whereas the final morphology of the crystals depends on the slow-growing planes.[26] The crystal structure of orthorhombic MoO_3 can be viewed as a layered structure that is parallel to {010} planes, and each layer involves two kinds of sub-layers (Fig. 3c). Both the sub-layers are constructed by corner-shared octahedra along [001] and [100], and stack together by sharing the edges of the octahedra along [010]. A much longer spacing exists between the {010} planes (perpendicular to [010]) resulting in a lower affinity, thus restraining the crystal growth along [010]. This would lead to the crystal growth rate of {001} > {100} ≫ {010} planes, which often occurs on naturally grown MoO_3 crystals of the orthorhombic type.[27] From another perspective, the equilibrium morphology of MoO_3 crystallites can be deduced in terms of the well-known Curie–Wulff construction.[28] In this regard, the distance (d_{hkl}) of a facet ($_{hkl}$) from the crystal's centre increases proportionally to its surface energy ($d_{hkl}/d'_{h'k'l'} = E_{\mathrm{surf}(hkl)}/E'_{\mathrm{surf}(h'k'l')}$). That is to say that the growth rates of the crystal facets are proportional to their surface energies. As a result, the most stable surfaces that possess the smallest d_{hkl} values dominate the overall shape of the crystallite. Correspondingly, the (010) surface of the MoO_3 crystallite should dominate the final equilibrium shape of "batten" according to the Wulff construction, and the (010) surface is the most stable in the as-formed MoO_3 "battens". Eventually, the as-formed "batten"-based hierarchical structure of MoO_3 was reduced to MoO_2 in hydrogen at 600 °C. As clearly displayed in Fig. 3d for

 This journal is © The Royal Society of Chemistry 2011

Published on 17 June 2011. Downloaded by Chinese University of Hong Kong on 26/09/2013 08:19:55.

the crystal model of orthorhombic MoO_3 projected along [001] and [100], a high density of O anions exist between the layers perpendicular to [010], and they could react with hydrogen easily. Compared with other directions in the layered structure, the chemical bonding along [010] are relatively weak and thus preferentially broken during the reduction process. Moreover, some defects such as oxygen deficiency and dislocation on the surface of MoO_3 crystals with relatively low activation energy could facilitate the hydrogen reduction. It is also important to note that reducing MoO_3 to MoO_2 causes a large volume shrinkage (about 37% as estimated by their bulk densities). The crystalline MoO_3 "battens" would collapse into fine MoO_2 grains in nanometre scales with numerous micro-/meso- pores between them (Fig. 4e and 4f). Interestingly, each assembly of MoO_2 nanocrystals still remains a similar shape to that of the parent MoO_3 "battens". Prompted by such unique secondary and complex nanoarchitectures of MoO_2, we expect that the as-formed hierarchically porous MoO_2 from our morphosynthesis would be beneficial as anode materials for lithium-ion batteries, because the existing nanoscale effects and macroscopic features would enhance the electrochemical lithium storage capabilities.

The lithium storage properties of the as-synthesized hierarchically porous MoO_2 sheet serving as a binder-free electrode were explored. Fig. 4a and 4b show the CV curves of the hierarchical MoO_2 electrode at a scan rate of 0.1 mV s^{-1} and at a voltage range of 0.01–3 V. It can be seen that there is a substantial difference between the first and subsequent cycles. In the first cycle, an irreversible broad peak centers at about 0.7 V during the cathodic discharge process, which can be associated with the irreversible reduction of electrolyte and the formation of a passivating surface film. In the subsequent cycles upon cycling, there exist two evident redox couples located at 1.53/1.74 V, and 1.23/1.50 V, respectively. They correspond to the reversible phase transitions (monoclinic–orthorhombic–monoclinic) of partially lithiated Li_xMoO_2 during lithium insertion and extraction, which agrees well with previous reports.[13c,14] The CV curves remain steady after the first cycle, indicating the highly reversible reduction and oxidation of this material. This may benefit from the unique hierarchical nanoarchitecture of MoO_2 with a network of interconnected hierarchical pores and inter-nanocrystallites. Fig. 4c shows the representative discharge and charge curves of the hierarchical MoO_2 electrode at a current density of 200 mA g^{-1} between 3.0–0.01 V *vs.* Li^+/Li. It is observed that the initial discharge/charge capacities are 587.2 and 506.3 mA h g^{-1}, respectively, and hence there is an irreversible capacity loss of 23.8%. No obvious potential plateau appears in the first cycle. From the second cycle onwards, however, two discharge plateaus at about 1.55 and 1.33 V and two charge plateaus at 1.42 and 1.69 V were clearly observed. As suggested by Dahn *et al.* and Shi *et al.*,[10c] the inflection point between these plateaus may be ascribed to phase transitions between the monoclinic phase and the orthorhombic phase in the partially lithiated Li_xMoO_2.

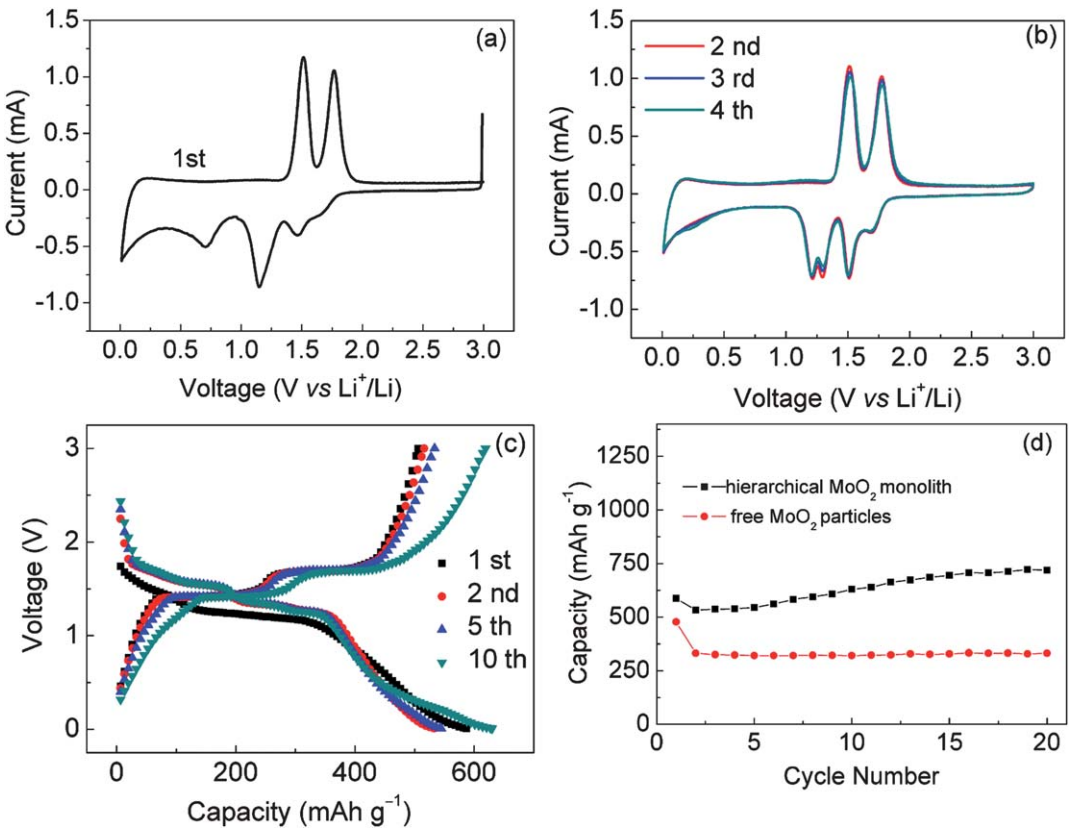

Fig. 4 (a,b) Cyclic voltammograms of hierarchically nanostructured MoO_2 at a scan rate of 0.1 mV s^{-1} in the voltage range of 3–0.01 V *vs.* Li. (c) Galvanostatic discharge and charge curves of hierarchically nanostructured MoO_2 electrodes cycled in the voltage range of 3–0.01 V *vs.* Li at a current density of 200 mA g^{-1}. (d) Cycling performance of the electrodes made of the hierarchical MoO_2 monolith and free MoO_2 particles in the voltage range of 3–0.01 V *vs.* Li at a current density of 200 mA g^{-1}.

Published on 17 June 2011. Downloaded by Chinese University of Hong Kong on 26/09/2013 08:19:55.

These phase transitions are highly reversible in the reduction and oxidation processes, in good agreement with the CV results. It is believed that the unique network of assembled nanocrystals and hierarchical inter-nanocrystallite porosity should contribute to the significant improvement in the electrochemical performance of hierarchically nanoarchitectured MoO_2, since it allows the electrolyte to be more accessible to all the surfaces of MoO_2 crystallites included in the electrode. Thereby, the Li diffusion kinetics is highly improved. This effect is similar to the already reported anodes of porous Si–C composites,[4a] TiO_2 nanosheet spheres,[4b] and mesoporous MoO_2.[14] In particular, the nanoscale dimension of inter-connected MoO_2 crystals renders the solid-state diffusion of Li^+ ions favorable. Another most distinctive advantage is that the inter-connected framework structure is expected to relieve well the local volumetric variation during the Li insertion/extraction reactions, thus enhancing the structural stability. Interestingly, the reversible capacity increases gradually upon cycling and reaches 719.1 mA h g^{-1}. This has been often observed in MoO_x-based electrode materials, possibly arising from the improved Li diffusion kinetics that was induced by an activation process associated with partial crystallinity degradation of the electrode to a disordered or amorphous-like structure during cycling.[14] As shown in Fig. 4d, the high reversible capacity of 719.1 mA h g^{-1} at 200 mA g^{-1} after 20 cycles is double that of the theoretical specific capacity of graphite (372 mA h g^{-1}). Also, it is important to note that high capacity and high reversibility without the special effort required for electron percolation such as carbon coating and without using any polymeric binder in the electrode are attractive features of our hierarchical MoO_2 anode. We envision that the electrode made of hierarchically nanostructured MoO_2 can be significantly improved by further optimization. As a comparison, we also studied the electrochemical properties of the MoO_2 particles (Fig. S7, See ESI†) prepared by the same two-step procedure of decomposition in air and reduction in 5% H_2/Ar without using any cotton template. The electrochemical performance of the electrode fabricated by mixing these free MoO_2 particles with carbon black and polymer binder (polytetrafluoroethylene, PTFE) is much worse than that of a binder-free hierarchically structured MoO_2 monolith (Fig. 4d and Fig. S9). Compared with the previously reported anodes based on MoO_2 nano-/micro-sized materials (*e.g.*, MoO_2 nanoparticles synthesized by reduction of MoO_3 with ethanol vapor: 318 mA h g^{-1} at 5.0 mA cm^{-2}; MoO_2 tremellas by a Fe_2O_3-assisted hydrothermal reduction of MoO_3: 600 mA h g^{-1} at 0.5 mA cm^{-2}; MoO_2/carbon hybrid nanowires converted from the organic-inorganic hybrid precursors: 595.7 mA h g^{-1} at 200 mA g^{-1}),[11a,12,13a] our electrode made of the binderless hierarchically structured MoO_2 monolith has a higher specific capacity.

Conclusions

In summary, a hierarchically nanostructured "cellulose" MoO_2 monolith has been successfully fabricated for the first time in large qualities through a simple morphogenetic process, whereby the cotton texture acts as both a template and a stabilizer. The unique hierarchical and complex architecture of assembled MoO_2 nanocrystals renders them flexible building blocks for advanced devices. Our preliminary results demonstrate that the MoO_2 monolith with hierarchical porosity and inter-connected framework is suitable for use as a binder-free anode in rechargeable lithium-ion batteries with both high specific capacity of 719.1 mA h g^{-1} and good reversibility. The as-formed single-component anode for lithium-storage devices benefits from the simplified fabrication process and reduced manufacturing cost, in comparison to conventional multi-component electrodes that are fabricated from a mixture of polymer binder and active material. We believe that the hierarchically nanostructured "cellulose" MoO_2 monolith would be an ideal candidate for elucidating the nanoarchitecture-dependent performance in sensing and catalytic applications, as well as in electrochromic displays.[4,8] The morphogenetic strategy in this study is facile but effective, and therefore it is very promising for cost-effective and large-scale industrial production. Future work is underway to improve both the electronic conductivity and reversible charge capacity at high current densities of hierarchical MoO_2 monoliths. Also, the facile morphosynthesis route could be extended to prepare other metal oxides with elaborate textural characteristics.

Acknowledgements

This work was supported by the Natural Science Foundation of China (Grant Nos. 50825203 and 51002057), the 863 program (Grant No. 2009AA03Z225), the Natural Science Foundation of Hubei Province (Grant No. 2008CDA026), the PCSIRT (Program for Changjiang Scholars and Innovative Research Team in University), and the Fundamental Research Funds for the Central Universities (HUST: 2010QN007). The authors thank Analytical and Testing Center of HUST for XRD, SEM, and TEM measurements.

Notes and references

1 (*a*) A. S. Arico, P. Bruce, B. Scrosati, J.-M. Tarascon and W. V. Schalkwijk, *Nat. Mater.*, 2005, **4**(5), 366; (*b*) L. X. Yuan, Z. H. Wang, W. X. Zhang, X. L. Hu, J. T. Chen, Y. H. Huang and J. B. Goodenough, *Energy Environ. Sci.*, 2010, **269**, 284.

2 (*a*) J. K. Kim and A. Manthiram, *Nature*, 1997, **390**, 265; (*b*) K. T. Nam, D. W. Kim, P. J. Yoo, C. Y. Chiang, N. Meethong, P. T. Hammond, Y. M. Chiang and A. M. Belcher, *Science*, 2006, **312**, 885; (*c*) P. Poizot, S. Laruelle, S. Grugeon, L. Dupont and J. M. Tarascon, *Nature*, 2000, **407**, 496; (*d*) F. Croce, G. B. Appetecchi, L. Persi and B. Scrosati, *Nature*, 1998, **394**, 456; (*e*) L. Taberna, S. Mitra, P. Poizot, P. Simon and J. M. Tarascon, *Nat. Mater.*, 2006, **5**, 567; (*f*) C. K. Chan, H. L. Peng, G. Liu, K. McIlwrath, X. F. Zhang, R. A. Huggins and Y. Cui, *Nat. Nanotechnol.*, 2007, **3**, 31; (*g*) Y. S. Hu, Y. G. Guo, W. Sigle, S. Hore, P. Balaya and J. Maier, *Nat. Mater.*, 2006, **5**, 713.

3 (*a*) Y. J. Lee, H. Yi, W. J. Kim, K. Kang, D. S. Yun, M. S. Strano, G. Ceder and A. M. Belcher, *Science*, 2009, **324**, 1051; (*b*) Y. Wang and G. Cao, *Adv. Mater.*, 2008, **20**, 2251; (*c*) Y. G. Guo, J. S. Hu and L. J. Wan, *Adv. Mater.*, 2008, **20**, 2878; (*d*) P. G. Bruce, B. Scrosati and J. M. Tarascon, *Angew. Chem., Int. Ed.*, 2008, **47**, 2930; (*e*) R. Z. Yang, Z. X. Wang, J. Y. Liu and L. Q. Chen, *Electrochem. Solid-State Lett.*, 2004, **7**, A496.

4 (*a*) A. Magasinski, P. Dixon, B. Hertzberg, A. Kvit, J. Ayala and G. Yushin, *Nat. Mater.*, 2010, **9**, 353; (*b*) J. S. Chen, Y. L. Tan, C. M. Li, Y. L. Cheah, D. Y. Luan, S. Madhavi, F. Y. C. Boey, L. A. Archer and X. W. Lou, *J. Am. Chem. Soc.*, 2010, **132**, 6124.

5 (*a*) H. X. Zhang, C. Feng, Y. C. Zhai, K. L. Jiang, Q. Q. Li and S. S. Fan, *Adv. Mater.*, 2009, **21**, 2299; (*b*) A. Abouimrane, O. C. Compton, K. Amine and S. T. Nguyen, *J. Phys. Chem. C*, 2010, **114**, 12800; (*c*) I. Lahiri, S. W. Oh, J. Y. Hwang, S. Cho, Y. K. Sun, R. Banerjee and W. Choi, *ACS Nano*, 2010, **4**, 3440; (*d*)

 This journal is © The Royal Society of Chemistry 2011

View Article Online

Published on 17 June 2011. Downloaded by Chinese University of Hong Kong on 26/09/2013 08:19:55.

X. F. Li, A. Dhanabalan, K. Bechtold and C. L. Wang, *Electrochem. Commun.*, 2010, **12**, 1222.

6 (*a*) S. Mann and G. A. Ozin, *Nature*, 1996, **382**(6589), 313; (*b*) H. Yang, N. Coombs and G. A. Ozin, *Nature*, 1997, **386**, 692; (*c*) G. A. Ozin, *Acc. Chem. Res.*, 1997, **30**, 17; (*d*) D. Volkmer, S. Tugulu, M. Fricke and T. Nielsen, *Angew. Chem., Int. Ed.*, 2003, **42**, 58.

7 (*a*) A. W. Xu, Y. R. Ma and H. Colfen, *J. Mater. Chem.*, 2007, **17**, 415; (*b*) A. W. Xu, M. Antonietti, H. Cölfenz and Y. P. Fang, *Adv. Funct. Mater.*, 2006, **16**, 903; (*c*) S. Mann, *Biomimetic Materials Chemistry*, VCH Publishers, Inc., New York, 1996; (*d*) S. Mann, *Angew. Chem. Int. Ed.*, 2000, **39**, 3393.

8 (*a*) K. Ariga, J. P. Hill, M. V. Lee, A. Vinu, R. Charvet and S. Acharya, *Sci. Technol. Adv. Mater.*, 2008, **9**, 014109; (*b*) K. Ariga, X. L. Hu, S. Mandal and J. P. Hill, *Nanoscale*, 2010, **2**, 198; (*c*) Q. M. Ji, S. Acharya, J. P. Hill, A. Vinu, S. B. Yoon, J. S. Yu, K. Sakamoto and K. Ariga, *Adv. Funct. Mater.*, 2009, **19**, 1792; (*d*) Q. M. Ji, S. B. Yoon, J. P. Hill, A. Vinu, J. S. Yu and K. Ariga, *J. Am. Chem. Soc.*, 2009, **131**, 4220.

9 (*a*) Y. J. Lee, Y. Lee, D. Oh, T. Chen, G. Ceder and A. M. Belcher, *Nano Lett.*, 2010, **10**, 2433; (*b*) M. Bengtsson, S. Ekstrom, J. Drott, A. Collins, E. Csoregi, G. Marko-Varga and T. Laurell, *Phys. Status Solidi A*, 2000, **182**, 495; (*c*) Y. Zhao, M. Wei, J. Lu, Z. L. Wang and X. Duan, *ACS Nano*, 2009, **3**, 4009; (*d*) J. Huang, X. Wang and Z. L. Wang, *Nano Lett.*, 2006, **6**(10), 2325; (*e*) Y. S. Nam, A. P. Magyar, D. Lee, J. W. Kim, D. S. Yun, H. Park, T. S. Pollom, D. A. Weitz and A. M. Belcher, *Nat. Nanotechnol.*, 2010, **5**, 340.

10 (*a*) C. F. Tsang and A. Manthiram, *J. Mater. Chem.*, 1997, **7**, 1003; (*b*) Y. G. Liang, S. J. Yang, Z. H. Yi, X. F. Lei, J. T. Sun and Y. H. Zhou, *Mater. Sci. Eng., B*, 2005, **121**, 152; (*c*) F. F. Ferreira, T. G. S. Cruz, M. C. A. Fantini, M. H. Tabacniks, S. C. de Castro, J. Morais, A. de Siervo, R. Landers and A. Gorenstein, *Solid State Ionics*, 2000, **136–137**, 357; (*d*) J. R. Dahn and W. R. McKinnon, *Solid State Ionics*, 1987, **23**, 1.

11 (*a*) L. C. Yang, Q. S. Gao, Y. Tang, Y. P. Wu and R. Holze, *J. Power Sources*, 2008, **179**(1), 357; (*b*) Y. G. Liang, S. J. Yang, Z. H. Yi, J. T. Sun and Y. H. Zhou, *Mater. Chem. Phys.*, 2005, **93**, 395; (*c*) Y. G. Liang, Z. H. Yi, S. J. Yang, L. Q. Zhou, J. T. Sun and Y. H. Zhou, *Solid State Ionics*, 2006, **177**, 501.

12 L. C. Yang, Q. S. Gao, Y. H. Zhang, Y. Tang and Y. P. Wu, *Electrochem. Commun.*, 2008, **10**, 118.

13 (*a*) Q. S. Gao, L. C. Yang, X. C. Lu, J. J. Mao, Y. H. Zhang, Y. P. Wu and Y. Tang, *J. Mater. Chem.*, 2010, **20**, 2807; (*b*) X. L. Ji, S. Herle, Y. H. Rho and L. F. Nazar, *Chem. Mater.*, 2007, **19**, 374; (*c*) Z. Y. Wang, J. S. Chen, T. Zhu, S. Madhavi and X. W. Lou, *Chem. Commun.*, 2010, **46**, 6906.

14 Y. F. Shi, B. K. Guo, S. A. Corr, Q. H. Shi, Y. S. Hu, K. R. Heier, L. Q. Chen, R. Seshadri and G. D. Stucky, *Nano Lett.*, 2009, **9**, 4215.

15 (*a*) L. A. Riley, S. H. Lee, L. Gedvilias and A. C. Dillon, *J. Power Sources*, 2010, **195**, 588; (*b*) S. H. Lee, Y. H. Kim, R. Deshpande, P. A. Parilla, E. Whitney, D. T. Gillaspie, K. M. Jones, A. H. Mahan, S. B. Zhang and A. C. Dillon, *Adv. Mater.*, 2008, **20**, 3627.

16 J. S. Chen, Y. L. Cheah, S. Madhavi and X. W. Lou, *J. Phys. Chem. C*, 2010, **114**, 8675.

17 (*a*) L. Q. Mai, B. Hu, W. Chen, Y. Y. Qi, C. S. Lao, R. S. Yang, Y. Dai and Z. L. Wang, *Adv. Mater.*, 2007, **19**, 3712; (*b*) V. M. Mohan, H. Bin and W. Chen, *J. Solid State Electrochem.*, 2010, **14**(10), 1769.

18 D. Mariotti, H. Lindström, A. C. Bose and K. Ostrikov, *Nanotechnology*, 2008, **19**(49), 495302.

19 (*a*) S. M. Paek, J. H. Kang, H. Jung, S. J. Hwang and J. H. Choy, *Chem. Commun.*, 2009, 7536; (*b*) Y. S. Kim, H. J. Ahn, H. S. Shim and T. Y. Seong, *Solid State Ionics*, 2006, **177**, 1323.

20 (*a*) K. O. Pope, M. E. D. Pohl, J. G. Jones, D. L. Lentz, C. von Nagy, F. J. Vega and I. R. Quitmyer, *Science*, 2001, **292**, 1370; (*b*) S. Frantz, G. A. Hubner, O. Wendland, E. Roduner, C. Mariani, M. F. Ottaviani and S. N. Batchelor, *J. Phys. Chem. B*, 2005, **109**, 11572.

21 (*a*) G. Rodriguez-Blanco, L. Giraldo and J. C. Moreno-Pirajan, *Appl. Surf. Sci.*, 2010, **256**, 5221; (*b*) P. N. Li, X. L. Hu, L. Zhang, H. X. Dai and L. Z. Zhang, *Nanoscale*, 2011, **3**, 974; (*c*) I. Isaev, G. Salitra, A. Soffer, Y. S. Cohen, D. Aurbach and J. Fischer, *J. Power Sources*, 2003, **119–121**, 28; (*d*) N. Kamath, J. S. Melo and S. F. D'Souza, *Appl. Biochem. Biotechnol.*, 1988, **19**, 251; (*e*) H. Yamazaki, R. K. H. Cheok and A. D. E. Fraser, *Biotechnol. Lett.*, 1984, **6**, 165.

22 (*a*) N. Albayrak and S. T. Yang, *Enzyme Microb. Technol.*, 2002, **31**, 371; (*b*) W. H. Scouten, *Methods Enzymol.*, **135**, 30.

23 J. F. Moulder, W. F. Stickle, P. E. Sobol and K. D. Bomben, *Handbook of X-ray Photoelectron Spectroscopy* (Ed: J. Chastain), Perkin-Elmer Corporation, Eden Prairie, MN, 1992.

24 (*a*) W. G. Klemperer and C. G. Wall, *Chem. Rev.*, 1998, **98**, 297; (*b*) M. Sadakane and E. Steckhan, *Chem. Rev.*, 1998, **98**, 219.

25 A. Ouriadov, B. Newling and S. N. Batchelor, *J. Phys. Chem. C*, 2008, **112**, 15860.

26 Y. G. Sun and Y. N. Xia, *Science*, 2002, **298**, 2176.

27 X. W. Lou and H. C. Zeng, *Chem. Mater.*, 2002, **14**, 4781.

28 (*a*) G. Wulff, *Z. Kristallogr*, 1901, **34**, 449; (*b*) J. Goclon, R. Grybos, M. Witko and J. Hafner, *J. Phys.: Condens. Matter*, 2009, **21**(9), 095008; (*c*) H. Schweiger, P. Raybaud, G. Kresse and H. Toulhoat, *J. Catal.*, 2002, **207**, 76.